Electronic Supplementary Material (ESI) for Integrative Biology

Supplementary figures:

1. Microfluidic device characteristics and cell compartmentalization

Microfluidic channels were molded in PDMS (Fig. S1 A and B) over silicon masters, which were structured with a two step DRIE process. The junction channels were fabricated through a masking area of 150 µm times 20 µm (Fig. S1 C1). After first etching step, they were 10 µm high. During 2nd etching step heights and lengths of the junction channel section were maintained, however, the cross section decreases through the down etching of the structures to finally obtain 100 µm deep microfluidic channels. DIC images clearly show borders of the main, side and junction channels (Fig. S1 C2). In fluorescent images, however, the under etching effect became visible, because proteins and fluorescent antibodies tended to stick to the PDMS surface (Fig. S1 C3). The reduced cross section of the junction channels increased the junction channel resistance, which helped to maintain gradients in the main area and prevented direct cell contact between astrocytes and neurons even more.

The major modification in our protocols to prevent direct cell contact between neurons and astrocytes, compared to neuronal cultures done before [1], was the side channel specific coating (Fig. S1 D1-5). While astrocyte channels were coated with 100 mg/ml poly(L-ornithine), neuron side channels and the main channel were coated only with 25 mg/ml poly(L-ornithine). The concentration difference between the astrocyte and main channel generated a gradient area mainly across the interlaced junction channels and partially in the main area close to the astrocyte side. The selective coating resulted in reduced neurite outgrowth and reduced branching of neurites in the main channel area towards the astrocyte side (Fig. S1 D4 versus S1 D5). Only sparsely neurite growth, entering the junction channels from the main channel side, was detected (Fig. S1 D6). Furthermore, those neurites were not observed to leave the junction channel into the astrocyte side.

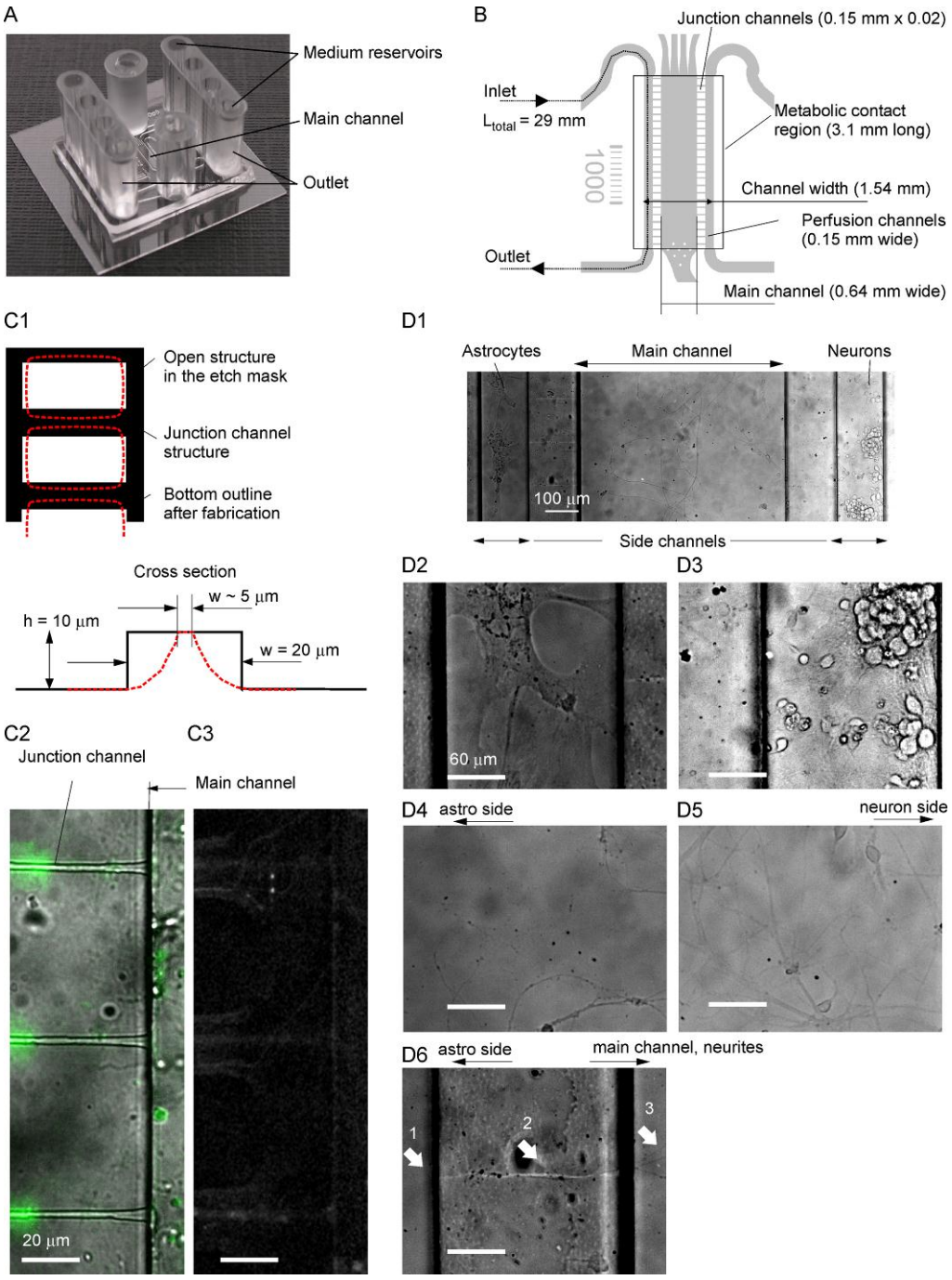

Suppl. figure S1: Further design specifications. (A) The picture shows the final PDMS device with incorporated PDMS reservoirs. (B) Microfluidic design with specified dimensions of specific cell culture regions. (C) Two-step fabrication process artifact. (C1) Mask area and final junction channel area in the silicon masters after cleanroom processing. (C2) DIC image shows top structure of junction channels. (C3) Fluorescent loaded junction channels appear larger in fluorescent images. (D1) DIC image of the metabolic contact area shows large distance (0.94 mm) between astrocyte and neuron culture channels. (D2, D3) Distinguishable astrocyte and neural cell morphology under DIC contrast. (D4, D5) Selective surface coating in the side and main channel reduces neurite outgrowth and branching towards the astrocyte cultures. (D6) Single representative neurite entered a junction channel (arrow 3) towards the astrocyte channel and remained in the junction channel (arrow 2 versus arrow 1).

2. Pressure driven flow in the side channels is based on selective liquid loading of the PDMS reservoirs of the microfluidic devices

During glutamate treatment, enriched medium was injected into the neuron channels, while media in the astrocyte channels remained pure. The concentration difference of glutamate in the side channels generated a concentration gradient across the main channel area. For easy cell handling and to avoid the use of syringe pumps in incubators, PDMS reservoirs were incorporated into the microfluidic chip (Fig. S1 A). Loading only on connected reservoir coursed a time variant flow through the microfluidic channel (Fig. S2 A and B). The flowrate decayed over time. As long as the side channel flowrate was faster than the diffusive flux through the junction channels the concentration gradient was maintained. By allowing a concentration difference (eq. 1) along the side channels of up to 10% (α = 0.9, eq. 2), flowrates may decrease down to ~ 0.1 nl/s (cutoff flowrate) in the side channels for small molecules (100 - 500 Da) with high diffusion coefficients (400 - 800 μm^2). Calculated values proposed constant gradients of glutamate under this condition for up to 1.5 h, however, experimental values reached the cutoff flowrate after about 1 h (Fig. S2 B). To understand time variance of gradients under changing flowrate conditions we developed a COMSOL model. The COMSOL model was validated through fluorescein gradient measurements (Fig. S2 C). To compare fluorescent gradients with simulated concentration profiles the following steps are needed: (1) Normalizing, (2) Converting and (3) Comparing (Fig. S2 D). Normalizing of intensity values was necessary, because fluorescent lamps often have inhomogeneous ultra violet intensity distribution and side wall effects may decrease detectable fluorescent signals. Fluorescent intensity values related to absolute concentrations through the Beer-Lambert law. We performed intensity measurements for fluorescein in the main channel with different concentrations (C [µM] = {5, 8, 13, 26, 30, 40, 50, 60, 70, 100}, Fig. S2 E1). Comparing experimentally achieved with computationally achieved concentration plots, for steady state condition in the main channel area, verified the usability of a COMSOL model for further experimental design (Fig. S2 E2 - E4). We tested in the COMSOL model the influence of different flowrates. Operating the microfluidic device at high flowrates (> 0.1 µl/s) in the side channels generated indeed crossflow through the junction channels that dominated gradient formation (Fig. S2 E5). Flowrates, however, relevant for our experiments are under 20 nl/s (22 nl/s for initial seconds) and were showing minor impact on the diffusive flux through the junction channels. For the same flowrate range, users can delay the injection of the 2nd reservoir up to 1 min (which is for every pipette trained user a very long time), which will cause a difference in flowrates between the side channels of 5 %, but not impact the gradient profile (Fig. S2 E6). Nevertheless, a flowrate difference between the side channels of 50 % impacted the gradient profile. Thus the flowrate in the side channels indeed influences gradient profiles in the main channel. For our operating flowrates, however, the effect can be neglected. Further details on gradient influencing parameters and equations were published in [2, 3].

$$\Delta C_{PerfCh} = C_{in} - C_{out} \qquad \text{eq.1}$$

$$C_{out} = \alpha C_{in} \qquad \text{eq. 2}$$

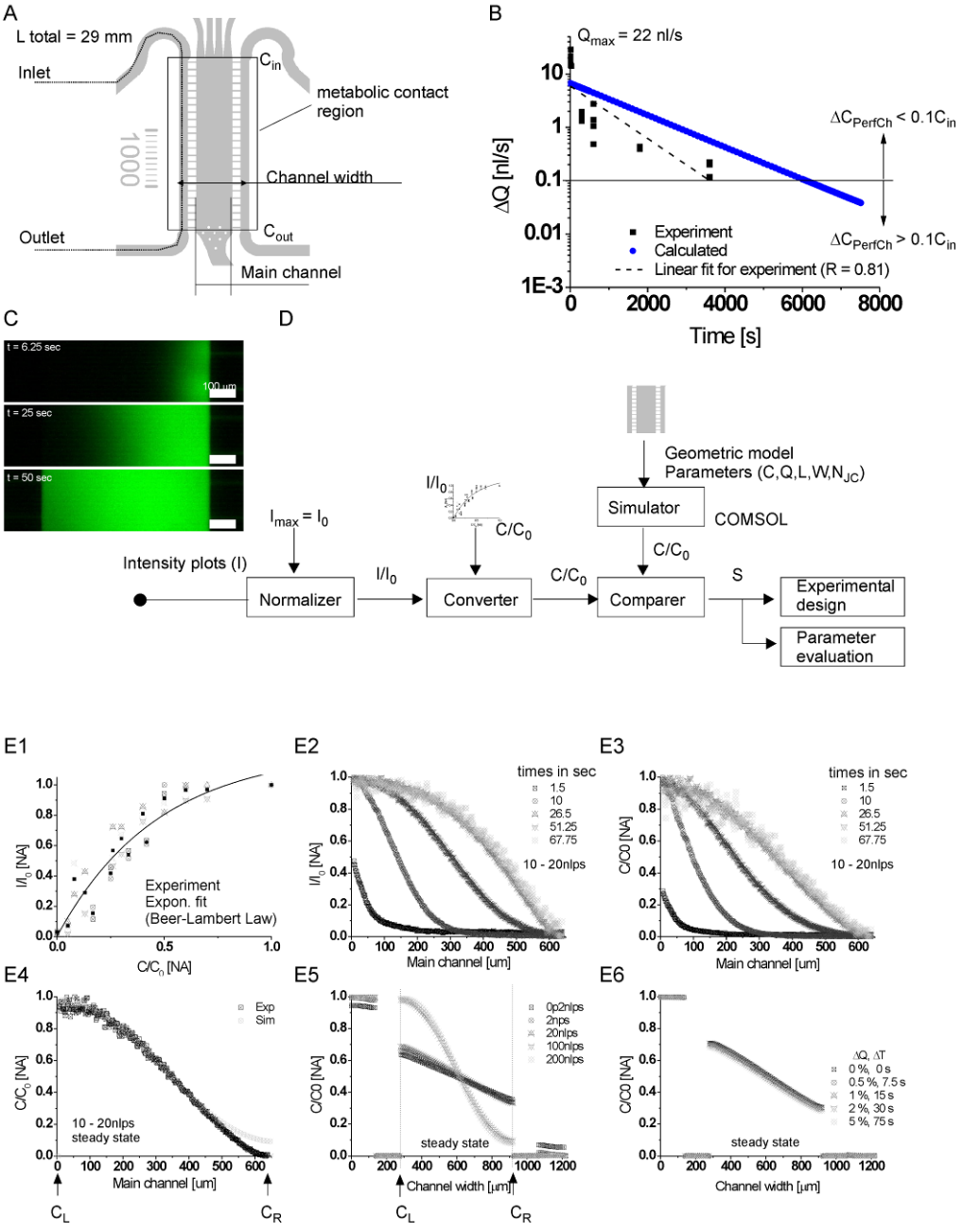

Suppl. figure S2: Flowrate and gradient formation in the microfluidic device under pressure driven flow. (A) Schematic of the microfluidic design with relevant regions for gradient formation across the main channel area. (B) Calculated and experimentally evaluated flowrates in the side channel induced through selective injection of liquid in one reservoir. (C) Fluorescein intensity measurements. (D) Validation process to establish a 2D COMSOL model for gradient formation in our microfluidic design. (E) Experimentally and computationally achieved intensity and concentration gradients in the metabolic area of the microfluidic device. (E1) Relationship between fluorescein concentration and intensity signal. (E2) Normalized intensity plots for fluorescein gradients. (E3) Converted fluorescein concentration gradients. (E4) Comparing experimentally and computationally concentration plots. (E5) Dependency of concentration profiles from flowrates in the side channels. (E6) Concentration profiles remain unchanged at flowrate differences generated through a delayed injection of about one minute.

Shear stresses in the side channels were calculated with the Haagen-Poisseuille equation and are 0.878 dyn/cm^2 (0.0878 N/m^2) for 22 nl/s and lower. Shear stress effects such as reduced cell viability or morphological changes have been reported for values larger than 0.26 N/m^2 [4] for non brain cells, so far. Here, we observed no morphological changes that might indicate shear stress effects in combination with transfection [5] or medium flushing during the glutamate treatment and washing cycles (Fig. S3).

3. Immunofluorescent characteristics of astrocytes in the microfluidic channels

Culturing cells, here astrocytes and neurons, in microfluidic channels and exposing them to fluid streams during the glutamate gradient treatment may affect (1) cell morphology, (2) cell metabolism and (3) cell function [6]. All three processes may impact the metabolic communication between astrocytes and neurons and thus influence non-cell autonomous effects in ALS. With figure S3 we can at least support that the cell morphology of astrocytes was not affected by their location in the microfluidic device (contact versus no contact region) and their exposure to medium flow during the three different experimental conditions.

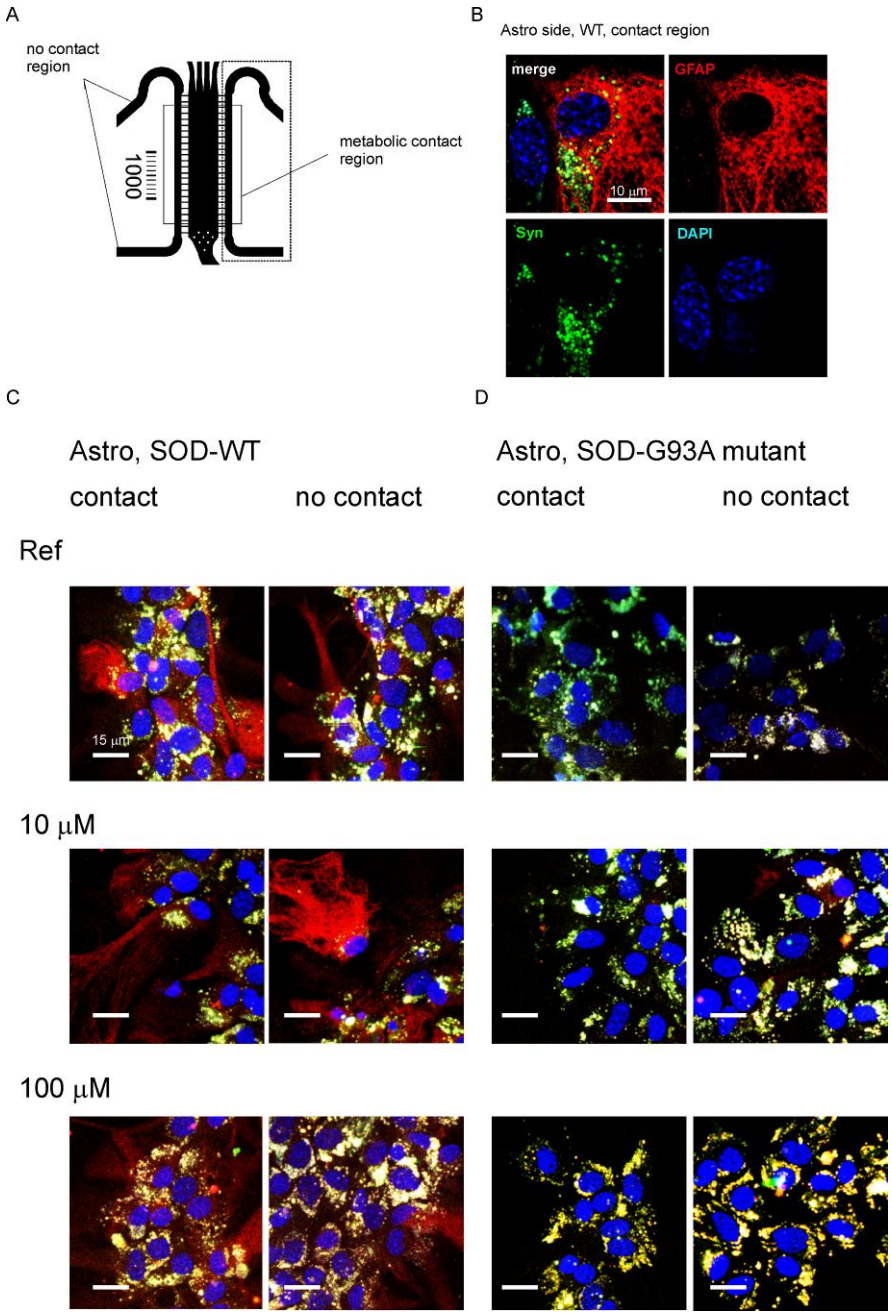

Suppl. figure S3: False colored confocal images of immunofluorescent labeled astrocytes in the microfluidic side channels. (A) Schematic of channel design highlights metabolic contract and “no contact” regions. (B) Single and merged colored images of the individual stainings against cell nucleus (DAPI, blue), astrocyte marker (GFAP, red) and axonal marker, presynaptic vessel protein (synaptophysin, green). Note that the overlap of synaptic vessel proteins (SYN) and GFAP results in false yellow color. Scale bar = 10 µm. (C) Confocal images of SOD-WT astrocytes in contact and “no-contact” region present no differences in cell morphology and GFAP expression. The homogeneous cell morphologies show no incidence of flow or cytotoxicity effects that may appear from perfusion of those cells during the glutamate treatment. Scale bar = 15 µm. (D) Confocal images of SOD-mutant astrocytes express lower GFAP expression, however, show no variation in morphology and GFAP expression under different experimental conditions and channel areas.

4. Immunofluorescent characteristics of astrocytes in the Petri dish

To characterize cell functionality after viral transfection of astrocytes, control experiments were performed in standard Petri dishes. Figure S4 shows astrocytes labeled against GFAP and synaptophysin (SYN). Similar to immunostaining results in the microfluidic device, astrocytes expressed GFAP and SYN markers (Fig S4 A1). Although synaptophysin is mostly known to be expressed by synaptic proteins located in neuronal axons, they also appear in astrocytes; however their appearance does not imply the co-localization of a neuronal axon (Fig. S4 A2). Moreover the appearance of synaptic proteins such as synaptophysin in astrocytes has already been reported, even *in situ* [7]. We have recognized, here, that omitting the primary antibody against synaptophysin, a green signal was still present, indicating small portions of background fluorescence from the cell culture (Fig. S2 A2 and S2 B2). This background signal, however, was much lower than in images with the primary antibody (Fig. S2 B1 and S2 C1) and was not observed in cultures with SOD-mutant transfection (Fig. S2 C2). Thus, the synaptophysin was specific to the astrocytes. Again similar to the results in the microfluidic channels, SOD-mutant astrocytes show reduced GFAP expression after viral transfection (Fig. S2 C1). We concluded that astrocyte morphology in the microfluidic devices was coherent with those in Petri dishes.

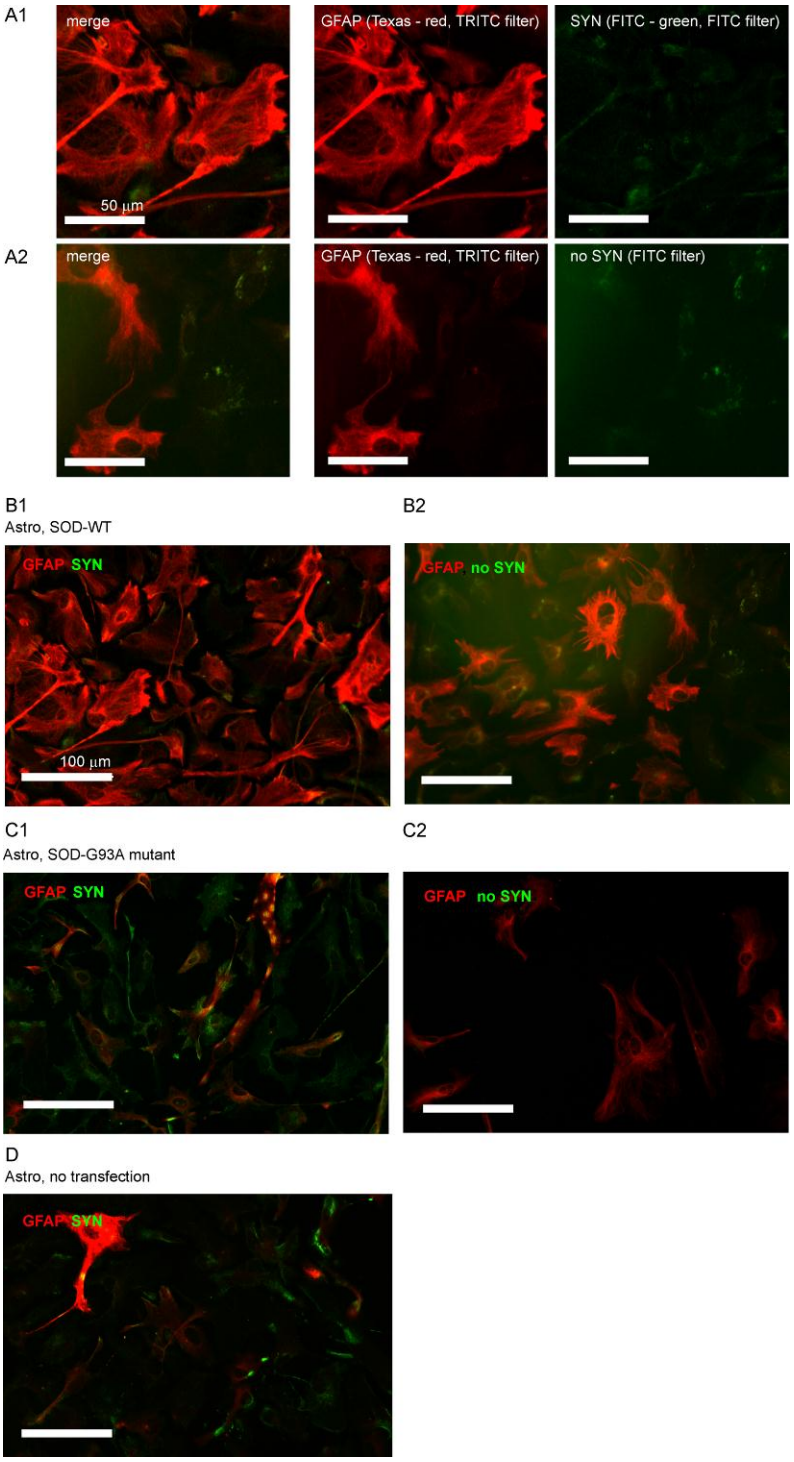

Suppl. figure S4: False colored confocal images of immunofluorescent labeled astrocytes in standard Petri dishes. (A) Single and merged colored images of the individual staining with (A1) both astrocyte marker (GFAP, red) and axonal marker, presynaptic vessel protein (synaptophysin, green), or (A2) with only GFAP. Note that the overlap of green and red signals results in false yellow color. Scale bar = 50 µm.
(B) False colored confocal images with SOD-Wt transfected astrocytes in Petri dish. (C) Mutant SOD-G92A transfected astrocytes after confocal imaging. (D) Untreated astrocyte monoculture after confocal imaging. Scale bar = 100 µm for (B-D).
(B1 and C1) Different GFAP expression occurred after viral transfection with SOD-WT and SOD-G93A. (B1, C1 and D) Synaptophysin expression remains in all cultures with or without different viral transfections.

References:

1. Kunze A, Meissner R, Brando S, Renaud P: **Co-pathological states of tau proteins in a 3D micropatterned neural cell culture**. In: *MicroTAS 2011: 2011; Seattle*; 2011.
2. Kunze A: **Micro-engineering the Cerebral Cortical Cell Niche: A new Cell Culture Tool for Neuroscience Research**. Lausanne: École polytechnique fédérale de Lausanne (EPFL); 2012.
3. Kunze A, Valero A, Zosso D, Renaud P: **Synergistic NGF/B27 Gradients Position Synapses Heterogeneously in 3D Micropatterned Neural Cultures**. *PLoS ONE* 2011, **6**(10):e26187.
4. Stathopoulos NA, Hellums JD: **Shear stress effects on human embryonic kidney cells in Vitro**. *Biotechnology and Bioengineering* 1985, **27**(7):1021-1026.
5. Shin HS, Kim HJ, Sim SJ, Jeon NL: **Shear Stress Effect on Transfection of Neurons Cultured in Microfluidic Devices**. *Journal of Nanoscience and Nanotechnology* 2009, **9**(12):7330-7335.
6. Millet LJ, Gillette MU: **New perspectives on neuronal development via microfluidic environments**. *Trends in Neurosciences* 2013, **35**(12):752-761.
7. Wilhelm A, Volknandt W, Langer D, Nolte C, Kettenmann H, Zimmermann H: **Localization of SNARE proteins and secretory organelle proteins in astrocytes in vitro and in situ**. *Neuroscience Research* 2004, **48**(3):249-257.